Target asymmetry measurement in $\gamma d \rightarrow pn$ at photon energies 300–700 MeV and partial wave analysis

Y. Ohashi,* N. Awaji,† H. Hayashii,‡ N. Horikawa, A. Miyamoto,§ T. Nakanishi, S. Okumi, H. Ozaki, and T. Tauchi§
Department of Physics, Nagoya University, Nagoya 464, Japan

T. Ishii, S. Kato, H. Okuno, and K. Ukai
Institute for Nuclear Study, University of Tokyo, Tanashi 188, Japan

K. Mori
Nagoya University College of Medical Technology, Nagoya 461, Japan

Y. Takeuchi§
Department of Applied Mathematics, Osaka University, Toyonaka 560, Japan
(Received 26 February 1987)

The polarized target asymmetry $T(\theta)$ for the reaction $\gamma d \rightarrow pn$ has been measured at proton c.m. angles of 70°, 100°, and 130° in the photon energy region between 300 and 700 MeV. The observed asymmetry shows relatively small values. A phenomenological partial wave analysis is carried out by using the present $T(\theta)$ data together with recent results on the differential cross section $d\sigma/d\Omega$, the recoil proton polarization $P(\theta)$, and the polarized beam asymmetry $\Sigma(\theta)$. The gross features of $d\sigma/d\Omega$, $T(\theta)$, and $\Sigma(\theta)$ are reproduced reasonably well without dibaryon resonances, but those of $P(\theta)$ are not, even with arbitrary smooth backgrounds in the present scheme of analysis. Possible contributions of dibaryon resonances are studied.

I. INTRODUCTION

Since the anomalous structure was observed in the difference between the p-p total cross sections for two longitudinal spin states (spin parallel and antiparallel) at Argonne National Laboratory,[1] the two-nucleon system has been investigated extensively in relation to the possible existence of dibaryon resonances. Several phase shift analyses[2,3] were made and several candidates of dibaryon resonances were proposed such as ${}^3F_3, {}^1D_2$ for I (isospin)$=1$ and ${}^1F_3$ for $I=0$.

The deuteron photodisintegration reaction $\gamma d \rightarrow pn$ is another important channel with information on both $I=1$ and 0 dibaryon states. In this reaction, an unexpectedly large proton polarization $P(\theta)$ was observed at $\theta_p^{\text{c.m.}}=90°$ for the photon energy around 550 MeV.[4,5] To explain this result, Ikeda *et al.*[5] performed a phenomenological analysis and concluded that it was impossible to reproduce the large polarization without introducing two dibaryon resonances, $I(J^P)=1(3^-)$ at 2260 MeV and $0(3^+)$ or $0(1^+)$ at 2380 MeV.

In addition to the accurate cross section measurements,[6–10] various polarization parameters such as the recoil proton polarization $P(\theta)$ (Refs. 4, 5, and 11–13), the polarized beam asymmetry $\Sigma(\theta)$ (Refs. 14–16), the polarized target asymmetry $T(\theta)$ (Refs. 17 and 18) and the double-polarization parameter $T_1(\theta)$ (Ref. 19) have been extensively measured. These polarization parameters have several important implications in clarifying the reaction mechanism.

(i) Predictions by the analysis above indicate that these parameters are sensitive to the inclusion of dibaryon resonance terms.

(ii) These provide important information towards the understanding of the reaction mechanism of $\gamma d \rightarrow pn$.

However, the previous data of $T(\theta)$ are not systematic enough to provide the crucial test for the inclusion of dibaryon resonances in this reaction channel. We have, therefore, measured $T(\theta)$ with better accuracy over wider energy and angular ranges, and carried out a phenomenological analysis using these data.

The present paper reports the measurement of $T(\theta)$ for the reaction $\gamma d \rightarrow pn$ at $\theta_p^{\text{c.m.}}=70°$, 100°, and 130° in the energy region between 300 and 700 MeV. This experiment was done at the 1.3 GeV electron synchrotron of the Institute for Nuclear Study (INS), the University of Tokyo. A letter on the experimental data has been published elsewhere.[20] In the present paper, details of the experiment are described together with the results of the analysis.

II. EXPERIMENTAL APPARATUS AND PROCEDURES

The layout of the experimental apparatus is shown in Fig. 1. A bremsstrahlung photon beam was incident on a polarized deuteron target. Protons in the reaction $\gamma d \rightarrow pn$ were detected with a magnetic spectrometer, and neutrons were detected with a scintillation counter array.

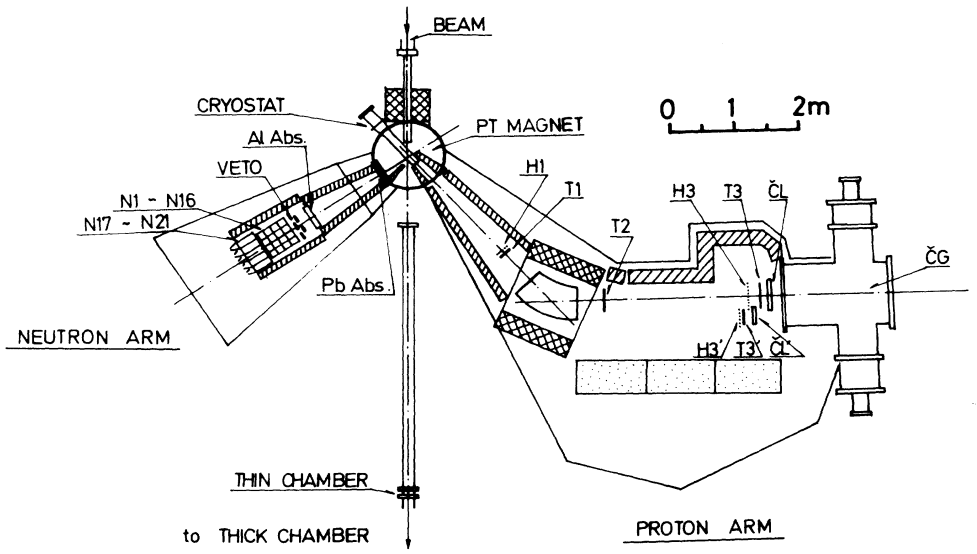

FIG. 1. Experimental layout. Trigger counters: T1, T2, T3 (T3'). Counter hodoscopes: H1, H3 (H3'). Čerenkov counters: CL (CL'), CG. Hatched area denotes lead blocks.

A. Photon beam

The bremsstrahlung photon beam was produced by the circulating electron beam of the synchrotron hitting an internal platinum radiator, 50 μm thick. The beam was collimated by two lead collimators with cross sections of 5.5×5.5 and of 5.7×5.7 mm^2 placed at 5.2 and 6.8 m from the radiator, respectively. The beam profile thus obtained was a square with a cross section of 15×15 mm^2 at the target position, 17.8 m downstream from the radiator. Two bending magnets behind the collimators swept out charged particles associated with the photon beam. The beam path between the second collimator and the polarized target was evacuated to reduce the background due to electromagnetic processes.

The beam intensity was measured by a thick-walled ionization chamber to an accuracy better than 3%. A thin-walled ionization chamber was set between the polarized target and the thick-walled chamber for use as a subsidiary beam monitor. The beam intensity was $(1 \sim 3) \times 10^9$ eq q/s with a duty factor of about 10% during the experiment.

B. Polarized deuteron target

The target material was 95% deuterated butanol (C_4D_9OD) and 5% deuterium oxide, doped with about 1% free radical (porphyrexide) by weight, in the form of frozen spheres of about 1 mm in diameter. The target beads were packed in a container made of 250 μm thick FEP (fluorinated ethylene propylene) film with a cross section of 20×20 mm^2 and a length of 40 mm. The typical filling factor of target beads was 0.65. The target material was cooled down to 0.5 K by means of a ^{3}He continuous-flow-type cryostat.[21] The deuterons in the target material were polarized by the dynamic method using microwaves of about 70 GHz in a uniform magnetic field of 2.5 T ($|\Delta B/B| < 2 \times 10^{-4}$ over the target volume). The deuteron polarization was measured continuously during the experiment by a fast-sweep Q-meter-type NMR system with a PDP 11/40 minicomputer.[22] The absolute value of the deuteron polarization was determined by detecting the thermal equilibrium (TE) signal at nearly 0.9 K and comparing it with the enhanced signal. A clean TE signal, as shown in Fig. 2, was obtained by averaging 20 000 sweeps after proper

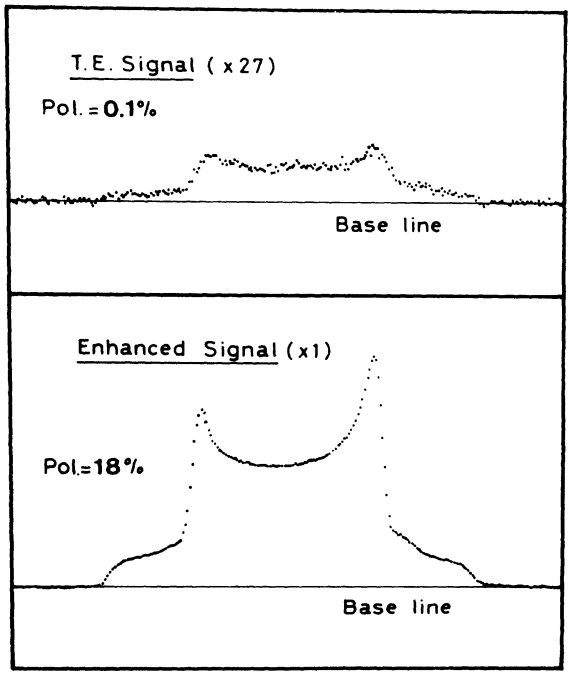

FIG. 2. NMR signals of deuterons. The thermal equilibrium (TE) signal averaged over 20 000 sweeps and the enhanced signal averaged over 1000 sweeps.

TABLE I. Uncertainties in evaluating the polarization of the deuteron target.

Accuracy in the measurement of the TE signal	0.04
Depolarization effect due to radiation damage	0.02
Contamination of dispersive parts	0.01
Drift of circuit	
(a) Difference between TE and enhanced signals	0.01
(b) Drift of the base line during the enhanced signal measurement	0.01
Target temperature	0.007
Total ($\Delta P/P$)	≤ 0.05

subtraction of the baseline and its drift with both hardware and software subtraction techniques.[22] The average polarization was nearly 17% during the experiment. As listed in Table I, the total uncertainty in the target polarization ($\Delta P_T/P_T$) was estimated to be about $\pm 5\%$, where the error in the measurement of the TE signal dominates.

The direction of polarization was reversed every 4–8 h to avoid possible systematic errors. Irradiation of the target by the photon beam caused a decrease in the polarization during data taking. When the polarization had decreased to about 90% of its initial value, the target material was annealed by raising its temperature to about 140 K for about 60 min. This was necessary when the total irradiation dose approached 5×10^{14} eq q.

The structure of the cryostat around the target container is shown in Fig. 3. In order to reduce the electromagnetic background, the cryostat walls on the beam path were made of thin material.

C. Detection system

The reaction $\gamma d \rightarrow pn$ was detected by observing coincidences between the proton and the neutron in the magnetic spectrometer and in the scintillation counter array, respectively.

The proton spectrometer consisted of a magnet, scintillation trigger counters (T1, T2, T3, T3′), counter hodoscopes (H1, H3, H3′), and Čerenkov counters (CG, CL, CL′). The angular acceptance was nearly 2 msr which was defined by the T1 counter. The spectrometer magnet had an entrance of 50 cm in width and 10 cm in height, and had a central orbit radius of 120 cm with a bending angle of 49.3°. The maximum field was 2.0 T, with a corresponding central momentum of 700 MeV/c. Particle trajectories were measured with three sets of hodoscopes H1, H3, and/or H3′ (H1, 12 strips of 80×20 mm^2; H3, 19 strips of 240×20 mm^2; H3′, seven strips of 240×30 mm^2). The angular resolution was about $\pm 0.8°$. The momentum resolution was about 1% for H3 and $\pm 1.5\%$ for H3′, and the total momentum acceptance was 23%. In high momentum (850 MeV/c) runs, the central-orbit radius was changed to 142.5 cm with the bending angle of 42.8° by shifting H3. In this case the total momentum acceptance was about 17%. Particle flight times were measured between T1 and T3 (or T3′) with a resolution of ± 0.5 ns, and the pulse height of T2 was measured. Positrons and positive pions were vetoed by the threshold Čerenkov counters; i.e., CG using freon-12 gas at the absolute pressure of 4.5 kg/cm^2

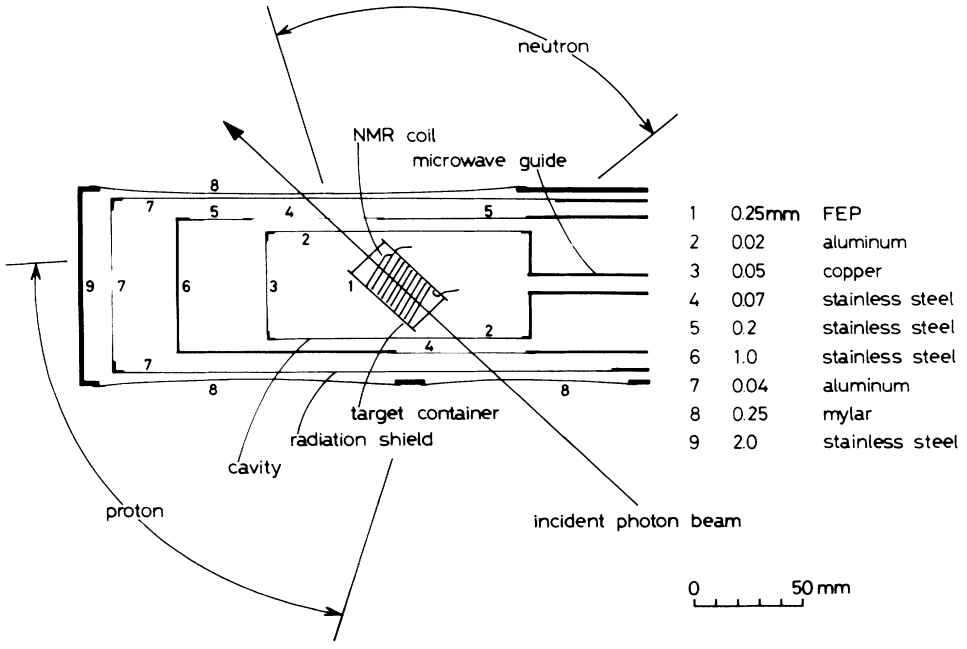

FIG. 3. The structure of the cryostat around the target.

($n=1.005$) and CL (CL') made of Lucite of 44 mm thickness ($n=1.49$).

Neutrons were detected by 21 blocks of plastic scintillator, each block having a cross section of 10×10 cm^2 and a length of 20 cm for N1–N16 and 30 cm for N17–N21. The scintillation counter array was set at a distance of 210 cm from the target point. The counters N1–N16 were placed vertically and N17–N21 were placed parallel to the scattered particles in the reaction plane. The gains of the photomultipliers were adjusted by use of momentum-analyzed electrons from a ^{90}Sr source and the neutron detection threshold was set to about 10 MeV for each counter.

To reduce the background events produced from materials other than the target, the neutron path was shielded by lead and concrete blocks. Serious sources of background were pair-created electrons and positrons in the target or in the cryostat walls. They were deflected and sprayed by the 2.5 T magnetic field, hitting the neutron counters. To avoid signal pileups in the neutron counters and to reduce the accidental coincidence rate, two kinds of absorbers were used, one was an aluminum plate 22 mm thick and the other was a lead plate 0–30 mm thick which attenuated neutrons by about 20% at maximum). Additional charged particles incident on the neutron counters were rejected by veto counters. The time difference between T1 and each neutron counter was measured, where constant fraction discriminators were used. The pulse height of each neutron counter was also measured. Gain drift of each photomultiplier was monitored by checking its pulse height with a light pulser, but no significant drift was observed during the measurement on each data point.

D. Electronic and data acquisition

The electronics logic was briefly as follows. A trigger signal P·N was generated by a coincidence between a signal P in the proton counters and a single N_i in any one of the neutron counters, in anticoincidence with the veto counters V:

$$P\cdot N=\sum_{i=1}^{21}(P\cdot N_i\cdot\overline{V})\ , \tag{1}$$

where

$$P=T1\cdot T2\cdot T3\cdot\overline{CG}\cdot\overline{CL}+T1\cdot T2\cdot T3'\cdot\overline{CL'}\ , \tag{2}$$

$$V=\sum_{i=1}^{21}(V_{2i-1}\cdot V_{2i})\ . \tag{3}$$

Two kinds of delayed triggers, $P_d\cdot N$ and $P\cdot N_d$, were also generated to monitor the rate of accidental events.

The trigger signal started the data acquisition cycle of the on-line computer. During this cycle, the following information was recorded: trigger logic pattern to distinguish the event type, hit patterns in all hodoscopes and in the neutron counters, the data of pulse heights and time of flights, integrated beam intensity, run parameters, and various scaler counts. These data for each event were registered in CAMAC modules and transferred to a PANAFACOM U-400 computer. The value of the target polarization sent from the PDP 11/40 minicomputer was also registered in the U-400 every 2 min. During the experiment, hit patterns, histograms, and spectra for each proton and neutron counter were displayed event by event on a monitor display of the U-400.

Every 76 events, the data (128 bytes/event) stored in the U-400 were transferred to the central computer FACOM M-180 IIAD via the INS on-line data acquisition system.[23] The tasks of the central computer were (i) to monitor the events by calculating the reaction kinematics and producing various histograms, and (ii) to store the data on a magnetic tape for further analysis.

III. DATA ANALYSIS

In the data analysis, events due to the reaction $\gamma d \rightarrow pn$ were selected from the background events by using parts of the detector information. Several corrections were applied in the extraction of the true yield from the polarized deuteron target.

A. Event analysis

The following criteria were required for the selection of $\gamma d \rightarrow pn$ events: (i) the trigger logic pattern was P·N, (ii) the only one counter was fired in each of the proton hodoscopes H1 and H3 (H3'), (iii) the pulse height of T2 and the time-of-flight between T1 and T3 (T3') counters were within a predetermined region corresponding to the proton, and (iv) at least one neutron signal had an appropriate pulse height and an appropriate time of flight. The contamination of positrons, positive pions, and deuterons in proton triggers was decreased to be less than 0.5% by condition (iii) as shown in Fig. 4. Ac-

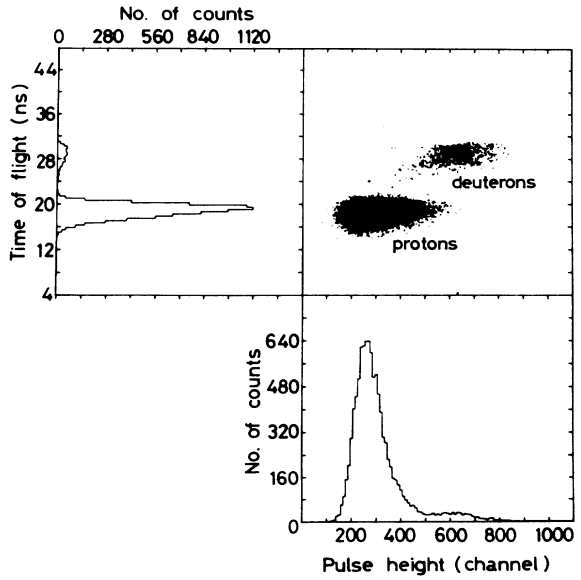

FIG. 4. Particle identification in the proton spectrometer. Pulse height of T2 and TOF between T1 and T3' ($\theta_p=100°$, $P_p=740\pm80$ MeV/c. The large peak in the spectrum corresponds to protons and the residual peak corresponds to deuterons.

cidental coincidences were successfully reduced to be less than 5% by condition (iv) as shown in Fig. 5, since accidental events had relatively small pulse heights. The remaining accidental events were subtracted by using the off-timing spectrum of the time difference, where the uncertainty associated with this subtraction is estimated to be less than 0.5% of true events.

Among the hit patterns of the hodoscopes, there were no-hit and multiple-hit events besides the normal single-hit events. The no-hit events were mainly due to the loss of particles in narrow gaps between the hodoscope counters. Their rates of 3–4 % were almost constant and independent of the target material. They were not analyzed since they had no effect on the result of the target asymmetry. The multiple-hit events were probably the true coincidence ones associated with one or more accidental particles. Their rates were 3–4 % depending on the spectrometer setting. The correction for the event loss by multiple hit was applied by multiplying an overall factor for each run; however, this had no significant effects on the target asymmetry.

The event loss due to inhibit time in the CAMAC data acquisition system was 6–9 %, which was corrected for each run.

B. Backgrounds

Two distinct processes can contribute to the background: (a) events from carbon and oxygen and nuclei in the polarized target, and (b) events from other processes (such as pion production) from polarized deuterons. The carbon and oxygen nuclei are not polarized, so that the background from those nuclei will only dilute true asymmetries. On the other hand, the background from the polarized deuterons can give false asymmetries.

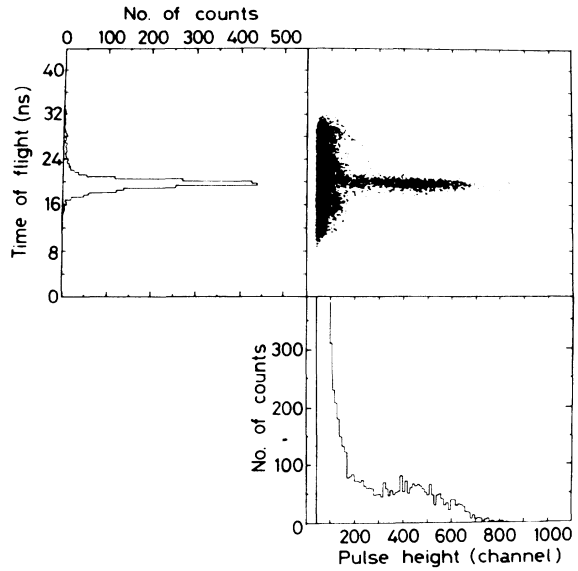

FIG. 5. Typical event distribution in the neutron detector. Pulse height of N12 and TOF between T1 and N12 ($\theta_p = 100°$, $P_n = 840 \pm 110$ MeV/c). TOF distribution is displayed against the events having pulse heights larger than the threshold used in the event analysis corresponding to the channel number of 250.

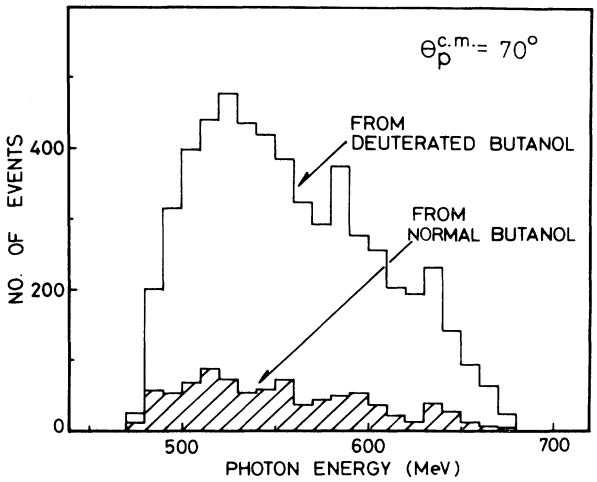

FIG. 6. Typical distribution of pn events from the polarized, deuterated butanol target and from the normal butanol target as a function of the photon energy, where the photon energy was calculated from the measured proton momentum by assuming two-body kinematics for the reaction $\gamma d \rightarrow pn$. The end-point energy of the bremsstrahlung beam was 700 MeV.

The background from the type (a) processes was subtracted by measuring P·N events from a dummy target of normal butanol (C_4H_9OH). The ratio of yields from normal butanol to those from deuterated butanol varied from 0.12 to 0.25 depending on data points. Typical events distributions for both kinds of target are plotted in Fig. 6.

As for type (b) background, the reaction $\gamma d \rightarrow pn\pi^0$ is considered to be the main source in our kinematical condition. For half the data points, the contribution from $\gamma d \rightarrow pn\pi^0$ was kinematically excluded by the proper choice of maximum photon energy. For the remaining half of the data points, it was impossible to eliminate this background only by the kinematical setting, but those background contributions should be much suppressed for the following reasons: (i) the events from the quasifree one-pion photoproduction process were not detected because of our detecting conditions (small solid angle for the proton arm and acceptances only for particles with momenta greater than 500 MeV/c for protons and 400 MeV/c for neutrons), and (ii) the contribution of other than the quasifree process was estimated to be less than 1% by phase space considerations.

IV. EXPERIMENTAL RESULTS

The target asymmetry of the process $\gamma d \rightarrow pn$ is defined using three kinds of differential cross sections $d\sigma_+$, $d\sigma_0$, and $d\sigma_-$ for the three deuteron spin states,

$$T = \frac{3}{2}\frac{1}{P_T}\frac{d\sigma_+ - d\sigma_-}{d\sigma_+ + d\sigma_0 + d\sigma_-} . \quad (4)$$

The subscript + denotes the deuteron spin direction in $\mathbf{k}\times\mathbf{p}$, where $\mathbf{k}$ is the momentum vector of the incident photon and $\mathbf{p}$ is that of the scattered proton.

A. Derivation of target asymmetry

In terms of the measured yields, the target asymmetry is given from Eq. (1) as follows:

$$T=\frac{D_+-D_-}{P_-(D_+-N)+P_+(D_--N)}\ , \tag{5}$$

where $P_{+(-)}$ is the absolute value of the average deuteron polarization for each spin direction; $D_{+(-)}$ and N represent the normalized yields from the polarized deuterated butanol and the normal butanol, respectively. In this expression, as we did not measure the yield from unpolarized deuterated butanol (defined as D), we use the approximation of $D\simeq(D_++D_-)/2$. This replacement corresponds to the neglect of an asymmetry caused by the tensor part of the deuteron polarization. In our case, however, due to the small values of vector polarization ($|P_{+(-)}|\lesssim 20\%$), the possible error introduced by this replacement is estimated at less than $\pm 1.8\%$. The statistical error T was estimated with the formula

$$(\Delta T)^2=(\Delta T_+)^2+(\Delta T_-)^2+(\Delta T_N)^2\ ,$$

where

$$\Delta T_\pm=\Delta D_\pm(D_--N)/A\ , \tag{6}$$

$$\Delta T_N=\Delta N(D_+-D_-)/A\ , \tag{7}$$

$$A=[P_-(D_+-N)+P_+(D-N)]^2/(P_++P_-)\ . \tag{8}$$

B. Uncertainties in target asymmetry

Possible sources of systematic uncertainty are summarized below and listed in Table II.

TABLE II. Uncertainties in the $T(\theta)$ measurement.

	$\Delta T/T$	ΔT
Uncertainty in the target polarization	<0.05	
Contribution from the tensor polarization	<0.018	
Uncertainty in the filling factor of the target	<0.013	
Contribution from liquid ^{3}He	0.009	
Uncertainty in estimating the electronics dead time		<0.007
Uncertainty in estimating the other correction factors		<0.016
Contribution from the background processes		<0.013
Total uncertainty	<0.055	<0.022

(i) Uncertainty in the target polarization: The error $\Delta T/T$ caused by the uncertainty in the measurement of deuteron polarization is estimated to be less than $\pm 5\%$.

(ii) Contribution from liquid ^{3}He: This contribution was not subtracted by the dummy target measurement, but it is estimated from the weight of liquid ^{3}He (at 0.5 K) relative to the deuterated butanol target. The error $\Delta T/T$ caused by this unsubtracted ^{3}He contribution is about $\pm 0.9\%$.

(iii) Uncertainty in the target filling factor: The filling factors have a possible difference of 10% at maximum between the deuterated and the normal butanol target. The error $\Delta T/T$ caused by neglecting this difference is about $\pm 1.3\%$.

(iv) Uncertainty caused by the replacement of D by $(D_++D_-)/2$: As mentioned in Sec. IV A, the error $\Delta T/T$ is estimated at less than $\pm 1.8\%$.

(v) Uncertainty caused by the dead time of trigger counters: instantaneous counting rates of these counters were 0.7 MHz at maximum when the duty factor of the beam was taken into account, and the resulting dead time was 1.3%. Since the variation of each counting rate was kept within 10% during the experiment, the error T caused by this variation is less than $\pm 0.7\%$.

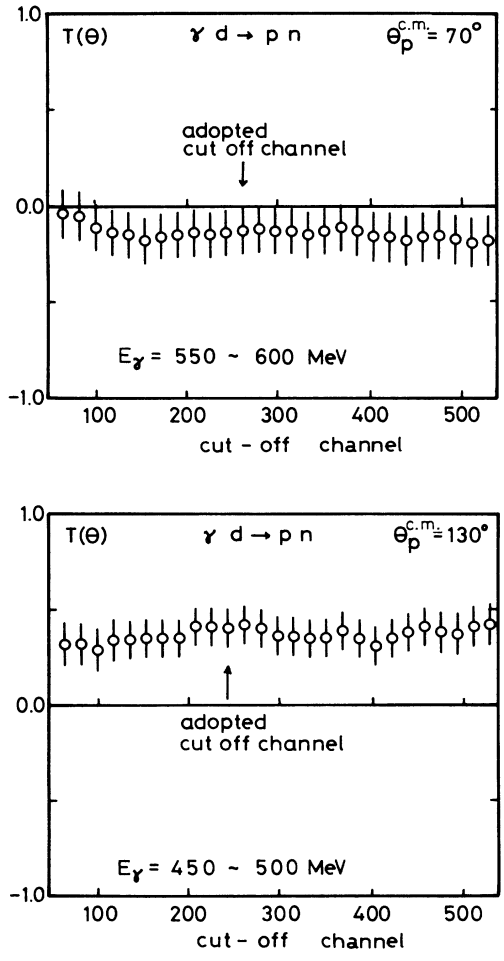

FIG. 7. Typical dependence of $T(\theta)$ on the cutoff value of pulse height in the neutron counters.

(vi) Uncertainty in the correction factor: The correction for the event loss due to multiple-hit events in hodoscopes, accidental events, and inhibit time of the CAMAC system had an overall uncertainty of 0.3%. The error ΔT is about $\pm 1.6\%$.

(vii) Uncertainty caused by background processes: As described in Sec. III B, this contamination to the true events is estimated to be less than 1%, and the resulting error ΔT is $\pm 1.3\%$ at maximum even if background processes have asymmetries of $\pm 100\%$.

A total systematic error (ΔT) becomes $\pm 8\%$ at maximum.

C. Some considerations on the reliability of $T(\theta)$

To assure the reliability of our $T(\theta)$ measurement, the following checks were made.

(a) As the pulse height spectrum of the neutron counter had continuous distribution as shown in Fig. 5, we set a cut level at a certain value above the background pulse height in the off-line analysis stage. The effect of the cut value on $T(\theta)$ was examined and typical results are shown in Fig. 7, where no remarkable dependence was seen over the wide range of the cut values.

(b) To check the effect of the background processes, the data were taken at different end-point energies of the bremsstrahlung beam. The results are consistent with each other within statistical errors.

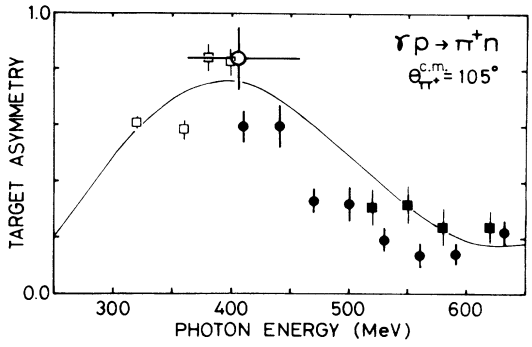

FIG. 8. Target asymmetry in $\gamma d \rightarrow \pi^+ n(n)$ at a π^+ c.m. angle of 105°. Data points are from Kharkov (Ref. 24) ( ), Daresbury (Ref. 25) ( ), Nagoya (Ref. 26) (100°,), and the present experiment ( ). The curve is the prediction by the phenomenological analysis of Arai and Fujii (Ref. 27) for the target asymmetry parameter in the $\gamma p \rightarrow \pi^+ n$ process.

(c) As a check of the whole detection system, we measured a target asymmetry of π^+ photoproduction from the polarized proton bound in a polarized deuteron (γ "p" $\rightarrow \pi^+ n$), detecting π^+ and n with the same apparatus. The measured data point was at the π^+ c.m. angle of 104° and a photon energy of 400 MeV, where a large asymmetry was expected. The result is in good agreement with the existing data[24–26] as shown in Fig. 8,

TABLE III. Results of the polarized target asymmetry in the reaction $\gamma d \rightarrow pn$. The errors are statistical only.

Photon energy bin (MeV)	Average photon energy (MeV)	Proton c.m. angle (deg)	Target asymmetry $T(\theta)$
320–350	337.1	72.0±1.9	−0.08±0.12
350–400	372.0	73.3±3.0	−0.14±0.11
400–450	424.9	71.5±3.2	−0.19±0.11
450–500	472.6	71.8±2.9	0.18±0.14
500–550	525.9	71.0±3.1	0.15±0.10
550–600	573.8	71.4±3.0	−0.14±0.12
600–650	623.4	72.6±2.2	−0.12±0.14
650–700	668.5	73.1±1.3	0.43±0.22
300–350	323.6	100.0±2.6	−0.02±0.10
350–400	371.6	101.6±2.9	−0.05±0.14
400–450	421.5	103.4±2.2	−0.04±0.26
470–500	486.6	98.3±2.7	−0.04±0.18
500–550	523.8	99.4±3.3	−0.02±0.16
550–600	573.6	100.8±3.0	0.11±0.18
600–650	621.6	101.7±2.6	−0.04±0.22
650–695	670.9	102.0±1.6	−0.16±0.53
330–350	342.4	129.9±2.8	0.02±0.23
350–400	377.1	130.2±2.9	0.34±0.14
400–450	423.7	130.4±3.0	0.14±0.16
450–500	474.7	130.0±2.9	0.36±0.09
500–550	522.5	130.3±3.0	0.21±0.11
550–600	572.1	130.7±2.9	−0.12±0.13
600–650	621.9	131.3±2.6	0.12±0.17
650–700	671.6	131.9±2.3	−0.18±0.30

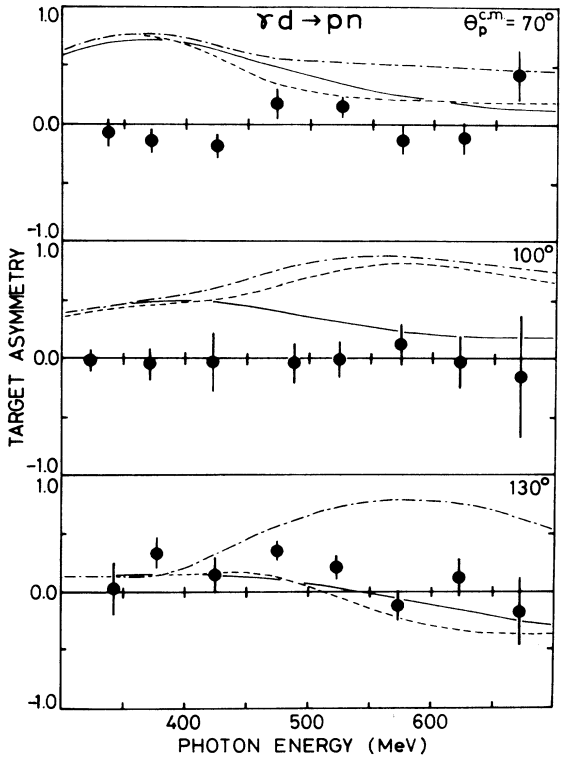

FIG. 9. Energy dependencies of the polarized target asymmetry $T(\theta)$ in γd→pn at θ_p=70°, 100°, and 130°. Curves are the predictions by Ikeda *et al.* (Ref. 5). The full curve corresponds to the solution without dibaryon resonances, the dashed curve includes the dibaryon resonances $1(3^-)$ at 2260 MeV and $0(1^+)$ at 2380 MeV, and the dash-dotted curve includes dibaryon resonances $1(3^-)$ at 2260 MeV and $0(3^+)$ at 2380 MeV.

and the reliability of the whole detection system including the polarized target system was assured.

D. Results

The experimental results for the target asymmetry are listed in Table III, and plotted in Fig. 9. As seen in Fig. 9, the $T(\theta)$ values are small and fluctuate around zero for all measured energies and angles, and no significant dependence on the incident photon energy is found. This features is remarkable, being in marked contrast to the proton polarization which has large values and shows a strong energy dependence in the same energy region.

The curves shown in Fig. 9 are the predictions of the phenomenological analysis made by Ikeda *et al.*[5] There is no solution which fits the present $T(\theta)$ data consistently at all energies and angles.

V. PHENOMENOLOGICAL ANALYSIS

The partial wave analysis of the reaction γd→pn was first done by Ikeda *et al.*[5] To explain the large proton polarization which is observed, they introduced dibaryon resonances. Recently, in addition to the present measurement on $T(\theta)$, several new measurements have been reported. Overall features of these new data are not reproduced by any solution of their analysis.

In order to check whether the disagreement between the data and their prediction is due to inappropriate parameters of dibaryon resonances or not, we tried to fit the data by adjusting the coupling parameters of the resonances, whereas the nonresonant amplitudes are unchanged. Results showed that the data could not be reproduced even if four dibaryon resonances were included. This suggested the necessity of revised treatment of the nonresonant amplitudes.

Therefore, we first examined the nonresonant amplitudes in detail. Next, the amplitudes of dibaryon resonances were superimposed on them.

A. Model

In the present analysis, the amplitudes of the reaction γd→pn is composed of following four terms: (1) the nucleon-exchange Born amplitudes [Fig. 10(a)], (2) the one-pion reabsorption amplitudes [Fig. 10(b)], (3) the additional background amplitudes, and (4) the dibaryon amplitudes [Fig. 10(c)]. Formulations of terms (1), (2), and (4) are the same as those ones represented by Ikeda *et al.*[5] The nucleon-exchange Born amplitudes were evaluated by adopting the dNN vertex function given by Wynn.[28] The one-pion reabsorption amplitudes were calculated by following Ogawa *et al.*,[29] where γN→πN part of the diagram was replaced by the phenomenological amplitudes of the single-pion photoproduction.

An additional background amplitude was introduced for each multipole transition amplitude, $E_L(^{2S+1}l_J)$ and $M_L(^{2S+1}l_J)$, where L, S, l, and J are the orbital angular momentum of the γd system, total spin, orbital angular momentum, and total angular momentum of the NN state. Forms of the background amplitude are discussed later.

We assumed that the dibaryon amplitudes have the following Breit-Wigner form:

$$E_L(^{2S+1}l_J) \text{ or } M_L(^{2S+1}l_L) = \exp(2i\gamma)\alpha\frac{\Gamma_1^{1/2}\Gamma_1^{1/2}}{W_0 - W - i\Gamma/2}\ , \quad (9)$$

with

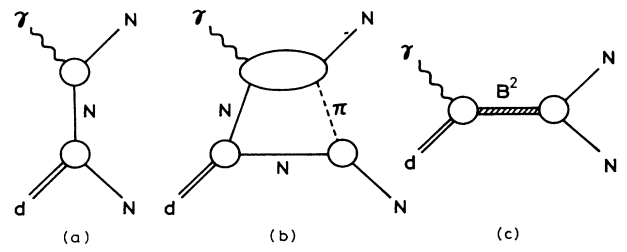

FIG. 10. Diagrams in the γd→pn. (a) Nucleon-exchange Born, (b) pion-reabsorption, and (c) dibaryon terms.

$$\Gamma_1=\tfrac{1}{2}\Gamma\left[\frac{k}{k_0}\right]^{2L}\left[\frac{k_0^2+x^2}{k^2+x^2}\right]^{L}, \tag{10}$$

$$\Gamma_2=\tfrac{1}{2}\Gamma\left[\frac{p}{p_0}\right]^{2l+1}\left[\frac{p_0^2+x^2}{p^2+x^2}\right]^{l}, \tag{11}$$

where k, p, W, Γ, and x are c.m. photon energy, c.m. nucleon momentum, total c.m. energy, total resonance width, and angular momentum barrier parameter, respectively. W_0 is the mass of the resonance, and k_0 and p_0 are the values of k and p at the resonance energy $W=W_0$. The coupling parameter and the phase parameter are denoted α and γ, which are to be determined by fitting the data.

B. Calculation without dibaryon resonances

For the first stage, we evaluated the amplitudes due to the nucleon-exchange Born term and the one-pion reabsorption term following the analysis by Ikeda *et al.*[5] The main contribution to $d\sigma/d\Omega$ comes from these terms and the results for $d\sigma/d\Omega$ agree with the data around 90°. However, above 400 MeV, the calculation shows a sharp rise in the cross section at forward angles, while the data become smaller. Hence, we searched for the amplitudes which reproduce the behavior of the data by modifying these terms in the following way.

(i) *The amplitudes for the single-pion photoproduction.* We calculated the one-pion reabsorption term with two different amplitude sets by Moorhouse *et al.*[30] and by the Nagoya group.[31] No remarkable difference was observed between the cross sections obtained by use of these two amplitude sets. We adopted those by the Nagoya group in the following calculation, because their analysis included more recent data.

(ii) *The deuteron wave function.* As for the effect of the deuteron wave function, we examined the wave functions given by Hulthén and Sugawara,[32] Lacombe *et al.*,[33] and Buck and Gross[34] to reproduce the $d\sigma/d\Omega$ data. We adopted the one by Lacombe *et al.* because it gave a relatively better fit to $d\sigma/d\Omega$ data at photon energies from 500 to 600 MeV.

(iii) *The vertex form factors.* In the present model, the amplitudes for the $\gamma N\rightarrow\pi N$ vertex in the one-pion reabsorption diagram are replaced by the ones for the real process $\gamma N\rightarrow\pi N$. The off-shell property of the exchanged pion was taken into account by using the following form factor,

$$h(t)=(\Lambda^2-m_\pi^2)/(\Lambda^2-t), \tag{12}$$

for the πNN and $\pi\Delta N$ vertices. We used cutoff parameters for the πNN and $\pi\Delta N$ vertices as $\Lambda_{NN}=880$ MeV and $\Lambda_{\pi\Delta N}=745$ MeV. Another cutoff parameter of a closed loop integral appearing in the calculation of the one-pion reabsorption diagram (it is referred as Λ_3 in Ref. 29) was chosen to be $\Lambda_{\rm cut}=265$ MeV. These values are also determined to fit the $d\sigma/d\Omega$ data.

With these modifications, we obtained the amplitudes which reproduced the $d\sigma/d\Omega$ data well without introducing any additional term and s-channel resonance term. However, $P(\theta)$, $\Sigma(\theta)$, and $T(\theta)$ data cannot be reproduced with these nonresonant amplitudes only.

In the second stage of the analysis, we tried to introduce additional background amplitudes to reproduce the spin parameters consistently. The constraints to the background amplitudes were as follows: (i) they should vary smoothly with energy, (ii) their magnitudes should be relatively small, (iii) they were all real, and (iv) they should be added only to low partial waves; namely to the dipole and quadrupole transition amplitudes with an NN orbital angular momentum of $l\leq 2$.

First, we examined various combinations of background multipoles with constant amplitudes. It is found that the $T(\theta)$, $\Sigma(\theta)$, and $d\sigma/d\Omega$ data are reproduced well by the introduction of at least three background multipoles, $E_1(^1P_1)=-200$ $\mu b^{1/2}$, $M_1(^3S_1)=-310$ $\mu b^{1/2}$, and $E_2(^3S_1)=400$ $\mu b^{1/2}$. However, the $P(\theta)$ data were not reproduced with any combination of constant backgrounds. The contribution of the above background amplitudes to the total cross section is less than 5% below 500 MeV, but a higher energies, it becomes larger. We also checked the fit to the data by trying background amplitudes which varied linearly with the photon energy, but no remarkable improvement was observed for $P(\theta)$.

C. Calculation with dibaryon resonances

The dibaryon amplitudes were superimposed on the above-mentioned nonresonant amplitudes which reproduced the $d\sigma/d\Omega, T(\theta)$, and $\Sigma(\theta)$ reasonably well. The resonance parameters α and γ were determined by the χ^2 fit to $d\sigma/d\Omega$, $T(\theta)$, $\Sigma(\theta)$, and $P(\theta)$ in the photon en-

TABLE IV. Data used in the fit with phenomenological models with dibaryon resonances.

	Institute	Reference	Number of data	Weight factor
$T(\theta)$	Tokyo	Present work	24	
	Bonn	Ref. 17	2	
	Bonn	Ref. 18	12	
		Total	38	2.50
$d\sigma/d\Omega$	Lund	Ref. 6	124	
	Tokyo	Ref. 8	50	
		Total	174	1.00
$P(\theta)$	Standford	Ref. 11	11	
	Bonn	Ref. 12	3	
	Tokyo	Ref. 4	8	
	Tokyo	Ref. 5	19	
	Kharkov	Ref. 13	40	
		Total	81	1.47
$\Sigma(\theta)$	Frascati	Ref. 14	4	
	Kharkov	Ref. 15	47	
		Total	51	1.85

ergy region from 300 to 700 MeV. The data used in the fit are listed in Table IV. The weighting factors were introduced to reduce the possible imbalance between the contributions to χ^2 among the different observables. Those were determined by taking into account the number of data for each observable, and given in Table IV.

At first, two dibaryon resonances, $1(2^+)$ at 2140 MeV and $1(3^-)$ at 2220 MeV, were introduced, which manifested themselves clearly in the pp elastic channel. The $d\sigma/d\Omega$, $T(\theta)$, and $\Sigma(\theta)$ data were reproduced rather well, while the results for $P(\theta)$ were not satisfactory. Although $P(\theta)$ data below 450 MeV were reproduced, those above 500 MeV were not. This result suggested the necessity of dibaryon resonances with higher masses if one wants to get better fits in the present scheme.

In the second step, we added one more dibaryon resonance to improve the fit to $P(\theta)$ at high energies. We considered the following three candidates: $1(4^+)$, $0(1^+)$, and $0(3^+)$. The first one was suggested from the investigation of the pp channel;[1] the others were from the study of the $\gamma d \rightarrow pn$ reaction.[5] We tested the following three combinations of resonances:

Solution A: $1(2^+)+1(3^-)+1(4^+)$,

Solution B: $1(2^+)+1(3^-)+0(1^+)$,

Solution C: $1(2^+)+1(3^-)+0(3^+)$,

The resulting parameters are listed in Table V and the results are shown in Fig. 11 together with the solution without dibaryon resonances. In these fits, we fixed the mass W_0, width Γ, and parameter x. The values of W and Γ are given in Table V, and x was taken to be 200 MeV/c. Although the overall fit to the data is still unsatisfactory, the gross structures of $P(\theta)$ are improved by the inclusion of these dibaryons.

D. Discussion on the results of the analysis

In Fig. 12, the angular dependence of $T(\theta)$ at 550 MeV (Ref. 18) is compared with results of the present analysis. Interpolated values of our data are also shown. Gross features of the angular dependence are reproduced reasonably well, but a detailed comparison between the three solutions is impractical.

In the present analysis, we have tried to fit the data on $d\sigma/d\Omega$, $T(\theta)$, $P(\theta)$, and $\Sigma(\theta)$ consistently by including the effect of two or three dibaryon resonances. By including three resonances, the overall fit improved, but discrepancies are still large for $P(\theta)$.

It should be noted that the present analysis contains some ambiguities in evaluating the nonresonant amplitudes: First, the subtraction of the photoproduction Born term from the phenomenological $\gamma N \rightarrow \pi N$ amplitudes was made to avoid the double counting of certain Feynman diagrams. This subtraction introduces an ambiguity in the evaluation of the $\gamma d \rightarrow pn$ amplitudes, because the Born amplitudes are not always a good approximation. Furthermore, we took into account only the one-pion reabsorption diagram, while it seems that the contribution of heavier mesons (such as ρ and ω) is not negligible in this energy region.

TABLE V. The results of the fits for the three hypotheses giving the smallest χ^2 values. The coupling parameter α is given in units of $\mu b^{1/2}$.

Solution A		Solution B		Solution C	
$1(2^+)$		$1(2^+)$		$1(2^+)$	
W_0	2140 MeV	W_0	2140 MeV	W_0	2140 MeV
Γ	100 MeV	Γ	100 MeV	Γ	100 MeV
γ	16°	γ	24°	γ	18°
$E_2(^1D_2)$	360	$E_2(^1D_2)$	288	$E_2(^1D_2)$	263
$M_1(^1D_2)$	−338	$M_1(^1D_2)$	−171	$M_1(^1D_2)$	−348
$M_3(^1D_2)$	−49	$M_3(^1D_2)$	85	$M_3(^1D_2)$	84
$1(3^-)$		$1(3^-)$		$1(3^-)$	
W_0	2220 MeV	W_0	2220 MeV	W_0	2220 MeV
Γ	120 MeV	Γ	120 MeV	Γ	120 MeV
γ	24°	γ	50°	γ	48°
$E_3(^3F_3)$	−57	$E_3(^3F_3)$	−12	$E_3(^3F_3)$	−80
$M_2(^3F_3)$	269	$M_2(^3F_3)$	223	$M_2(^3F_3)$	97
$M_4(^3F_3)$	−71	$M_4(^3F_3)$	44	$M_4(^3F_3)$	110
$1(4^+)$		$0(1^+)$		$0(3^+)$	
W_0	2430 MeV	W_0	2350 MeV	W_0	2350 MeV
Γ	160 MeV	Γ	200 MeV	Γ	200 MeV
γ	−3°	γ	−2°	γ	−5°
$E_4(^1G_4)$	−182	$E_2(^3S_1)$	258	$E_2(^3D_3)$	113
$M_3(^1G_4)$	−180	$E_2(^3D_1)$	−3	$E_2(^3G_3)$	−60
$M_5(^1G_4)$	40	$M_1(^3S_1)$	91	$E_4(^3D_3)$	−4
		$M_1(^3D_1)$	−60	$E_4(^3G_3)$	47
				$M_3(^3D_3)$	158
				$M_3(^3G_3)$	20

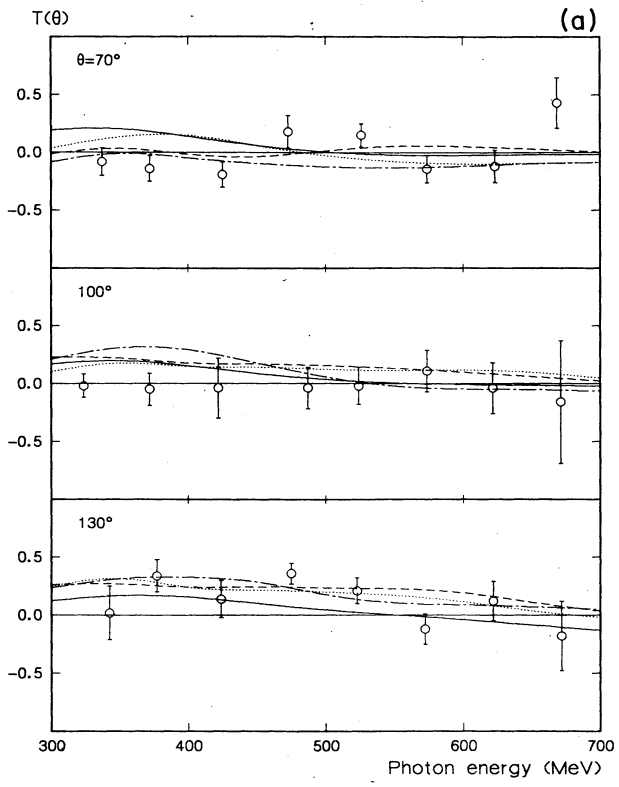

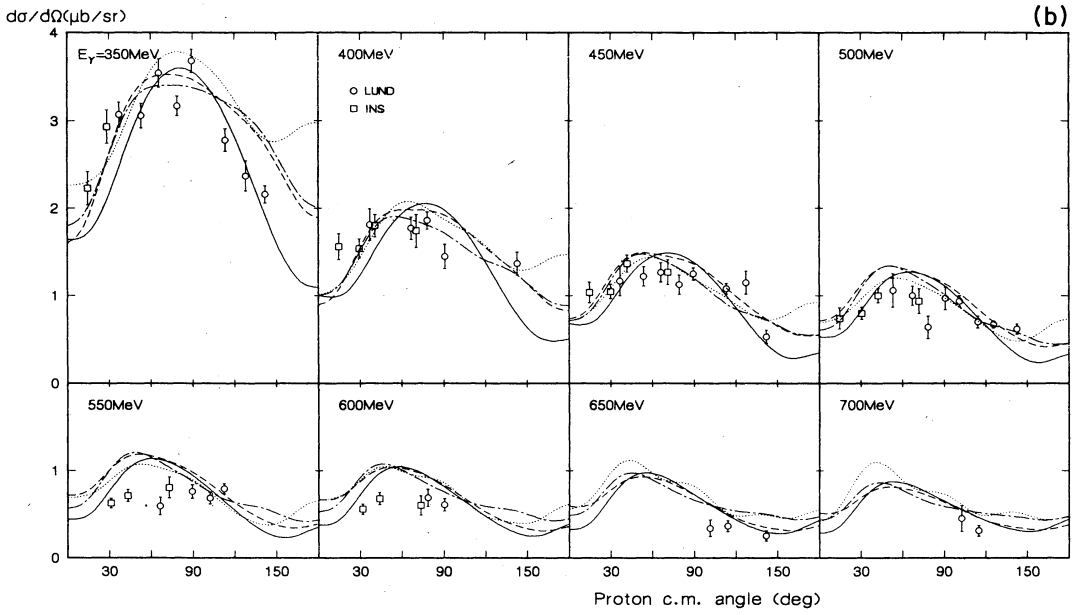

FIG. 11. Results of the phenomenological analysis. (a) Energy dependence of the polarized target asymmetry $T(\theta)$, (b) the angular distribution of the differential cross section $d\sigma/d\Omega$, (c) the recoil proton polarization $P(\theta)$, and (d) the polarized beam asymmetry $\Sigma(\theta)$. Solid lines in the figures show the results without dibaryon resonances; and dotted, dashed, and dash-dotted lines correspond to solutions A, B, and C shown in Table V. Data used in the fits are listed in Table IV.

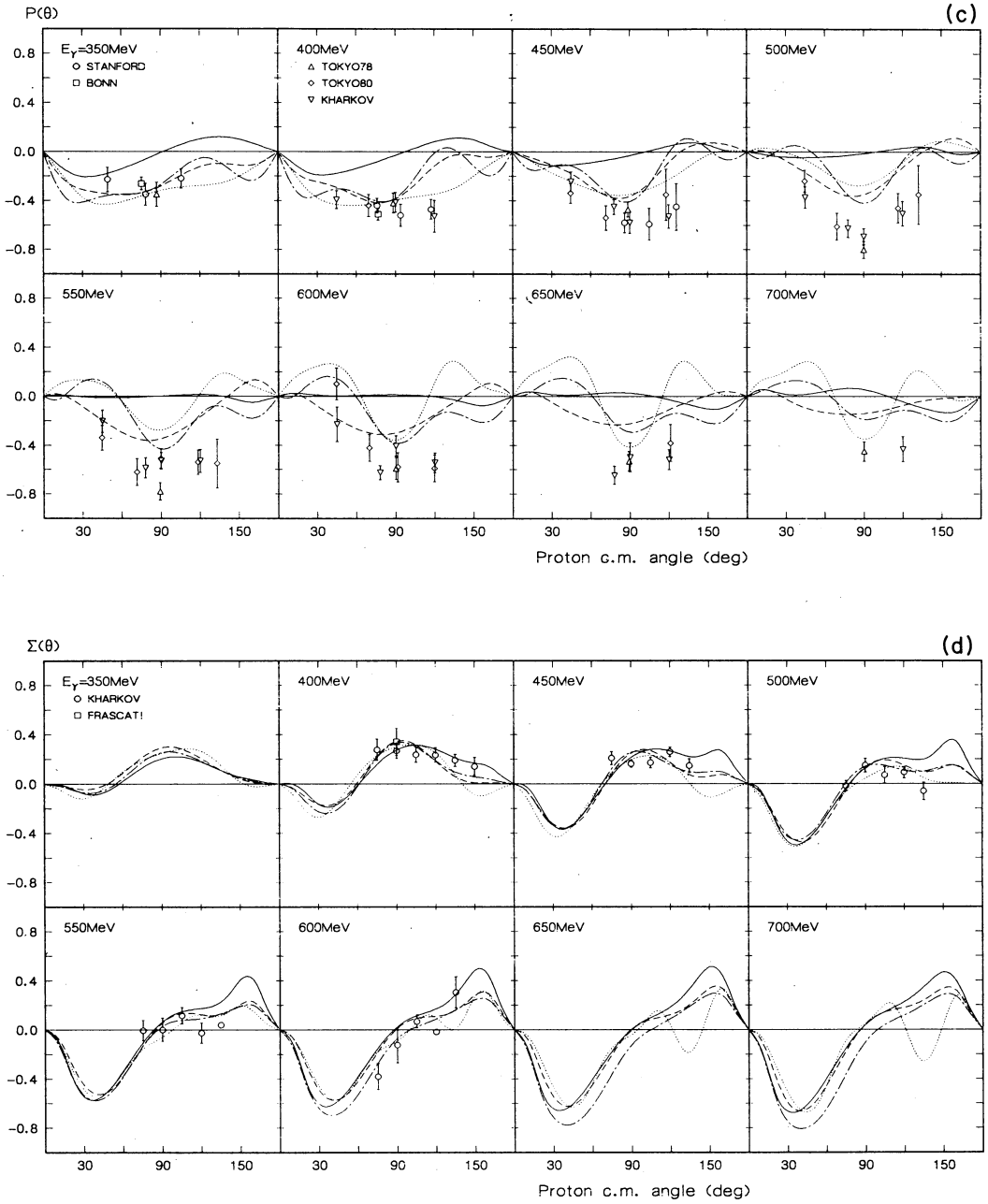

FIG. 11. (*Continued*).

Because of the above nature of the analysis, the nonresonant amplitudes calculated with the nucleon-exchange Born term and the one-pion reabsorption term have some uncertainty in low partial waves. This is the main reason for the introduction of the additional background term. Considering the fact that $\Sigma(\theta)$ and $T(\theta)$ are reproduced rather well and the fit to $d\sigma/d\Omega$ is partly improved by including the background, the major part of the discrepancy seems to be reduced by the background amplitudes given in Sec. V B.

Other theoretical analyses were made for the reaction $\gamma d \rightarrow pn$ by Laget,[35] Anastasio and Chemtob,[36] Huneke,[37] and Kisslinger and Cheung.[38] All these analyses indicated that the large $P(\theta)$ data cannot be reproduced without dibaryon resonances. These are in agreement with the present results.

Recently, Leidemann and Arenhovel[39] calculated various observables of the reaction $\gamma d \rightarrow pn$ by treating the final state interaction in a coupled channels approach with inclusion of Δ degrees of freedom. They have shown that $P(\theta)$ is very sensitive to the proper treatment of Δ and better agreement with the experimental data can be obtained. However, they could not fit the cross section data at the same time.

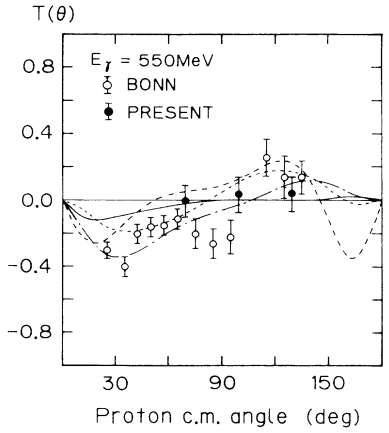

FIG. 12. Angular distribution of the polarized target asymmetry at $E_\gamma = 550$ MeV. Data are from Ref. 18 ( ) and interpolated values of the present data ( ). Curves in the figure correspond to those in Fig. 11.

VI. CONCLUSION

In conclusion, we have measured the target asymmetry $T(\theta)$ for the reaction $\gamma d \rightarrow pn$ in the photon energy range between 300 and 700 MeV at proton c.m. angles of 70°, 100°, and 130°. The values of $T(\theta)$ are small and no significant structure is found in the energy dependence of $T(\theta)$, in contrast to that of $P(\theta)$.

Using the present $T(\theta)$ data together with the $d\sigma/d\Omega$, $P(\theta)$, and $\Sigma(\theta)$ data, we have made a partial wave analysis. The results are summarized as follows:

(i) The $d\sigma/d\Omega$ data can be reproduced with the nucleon-exchange Born term and one-pion reabsorption term.

(ii) The gross features of the $\Sigma(\theta)$ and $T(\theta)$ data can be reproduced by the addition of the constant background amplitudes.

(iii) The behavior of the $P(\theta)$ data cannot be reproduced by the nonresonant amplitudes only, even if additional monotonic background amplitudes are assumed.

(iv) The $P(\theta)$ data can be explained by the introduction of dibaryon resonances. Two resonances, $1(2^+)$ and $1(3^-)$, are not sufficient to explain the large recoil proton polarization. Inclusion of three dibaryon resonances can improve the fit, but the agreement is still unsatisfactory.

For further study on dibaryon resonances in the reaction $\gamma d \rightarrow pn$, it is important to investigate the nonresonant amplitudes. For this purpose, systematic accumulation of various types of experimental data is necessary. In particular, high precision measurements of $d\sigma/d\Omega$ and $P(\theta)$ covering all angles are desired.

ACKNOWLEDGMENTS

We are especially indebted to Professor R. Kajikawa and Professor K. Morimoto for their encouragement and support in performing this experiment. We wish to thank the INS Electron Synchrotron crew and the INS High-Energy Group for their support during this experiment. We also thank the staff of the INS Computer Center, where the on-line data taking and the entire numerical analysis were carried out using the M180IIAD and the INS on-line data acquisition system. One of us (Y.O.) wishes to thank the Toyota Physical and Chemical Research Institute for financial support. One of us (Y.T.) also thanks the Japan Society for the Promotion of Science for financial support.

*Present address: Argonne National Laboratory, Argonne, IL 60439.
†Present address: Fujitsu Limited, Kanagawa, 211, Japan.
‡Present address: Nara Women's University, Nara 630, Japan.
§Present address: National Laboratory for High Energy Physics, Tsukuba, Ibaraki 305, Japan.

[1]A. Yokosawa, Phys. Rep. **64**, 47 (1980), and references therein.
[2]H. Hidaka *et al.*, Phys. Lett. **70B**, 479 (1977).
[3]N. Hoshizaki, Progr. Theor. Phys. **58**, 716 (1977); **60**, 1796 (1978); **61**, 129 (1979) (for $I=1$); K. Hashimoto and N. Hoshizaki, *ibid.* **64**, 1693 (1980) (for $I=0$).
[4]T. Kamae and T. Fujita, Phys. Rev. Lett. **38**, 468 (1977); T. Kamae *et al.*, Nucl. Phys. B **139**, 394 (1978).
[5]H. Ikeda *et al.*, Phys. Rev. Lett. **42**, 1321 (1979); Nucl. Phys. **B172**, 509 (1980).
[6]P. Dougan *et al.*, Z. Phys. A **276**, 55 (1976).
[7]J. Arends *et al.*, Nucl. Phys. **A412**, 509 (1981).
[8]K. Baba *et al.*, Phys. Rev. Lett. **48**, 729 (1982); Phys. Rev. C **28**, 286 (1983).
[9]K. H. Althoff *et al.*, Z. Phys. C **21**, 149 (1983).
[10]E. De Sanctis *et al.*, Phys. Rev. C **34**, 413 (1986).
[11]F. F. Liu, D. E. Lundquist, and B. H. Wiik, Phys. Rev. **165**, 1478 (1968).
[12]R. Kose *et al.*, Z. Phys. **220**, 305 (1969).
[13]A. S. Bratashevskij *et al.*, Yad. Fiz. **32**, 418 (1980) [Sov. J. Nucl. Phys. **32**, 216 (1980)].
[14]G. Barbiellini *et al.*, Phys. Rev. **154**, 988 (1967).
[15]V. G. Gorbenko *et al.*, Nucl. Phys. **A381**, 330 (1982).
[16]F. V. Adamian *et al.*, Czech. J Phys. B **36**, 945 (1986).
[17]K. H. Althoff *et al.*, Universität Bonn Report BONN-IR-80-33, 1980; G. Glasmachers, Universität Bonn Report BONN-IR-79-22, 1979.
[18]G. Anton, Universität Bonn Report BONN-IR-83-8, 1983.
[19]V. P. Barannik *et al.*, Nucl. Phys. **A451**, 751 (1986).
[20]T. Ishii *et al.*, Phys. Lett. **110B**, 441 (1982).
[21]M. Fukushima *et al.*, Nucl. Instrum. Methods **140**, 275 (1977); N. Horikawa *et al.*, Nagoya University Report DPNU-11-79, 1979.
[22]H. Hayashii *et al.*, Nagoya University Report DPNU-17-81, 1981.
[23]J. Kokame *et al.*, Nucl. Instrum. and Methods **213**, 317 (1983).
[24]V. A. Get'man *et al.*, Nucl. Phys. **B188**, 397 (1981).
[25]P. J. Bussey *et al.*, Nucl. Phys. **B154**, 205 (1979).
[26]M. Fukushima *et al.*, Nucl. Phys. **B130**, 486 (1977).

[27]I. Arai and H. Fujii, Nucl. Phys. **B194**, 251 (1982).
[28]W. M. Wynn, Ph.D. thesis, Georgia Institute of Technology, 1971.
[29]K. Ogawa, T. Kamae, and K. Nakamura, Nucl. Phys. **A340**, 451 (1980).
[30]R. G. Moorhouse, H. Oberlack, and A. H. Rosenfeld, Phys. Rev. D **9**, 1 (1974).
[31]K. Fujii *et al.*, Nucl. Phys. **B197**, 365 (1982).
[32]L. Hulthén and M. Sugawara, *Handbuch der Physik* (Springer-Verlag, Berlin, 1957), Vol. 39, p.1.
[33]M. Lacombe *et al.*, Phys. Lett. **101B**, 139 (1981).
[34]W. W. Buck and F. Gross, Phys. Rev. D **20**, 2361 (1979).
[35]J. M. Laget, Nucl. Phys. **A312**, 265 (1978).
[36]M. Anastasio and M. M. Chemtob, Nucl. Phys. **A364**, 219 (1981).
[37]H. Huneke, Diploma Thesis, Universität Bonn Report BONN-IR-80-24, 1980.
[38]C. Y. Cheung and L. S. Kisslinger, private communication.
[39]W. Leidemann and H. Arenhövel, Can. J. Phys. **62**, 1036 (1984); Phys. Lett. **139B**, 22 (1984).